HHS Public Access

Author manuscript

Nat Struct Mol Biol. Author manuscript; available in PMC 2015 July 01.

Published in final edited form as:

Nat Struct Mol Biol. 2015 January ; 22(1): 73–80. doi:10.1038/nsmb.2930.

THE AAA3 DOMAIN OF CYTOPLASMIC DYNEIN ACTS AS A SWITCH TO FACILITATE MICROTUBULE RELEASE

Mark A. Dewitt[1], **Caroline A. Cypranowska**[2], **Frank B. Cleary**[1], **Vladislav Belyy**[1], and **Ahmet Yildiz**[2,3,*]

[1]Biophysics Graduate Group, University of California, Berkeley CA, USA

[2]Department of Molecular and Cell Biology, University of California, Berkeley CA, USA

[3]Physics Department, University of California, Berkeley CA, USA

Abstract

Cytoplasmic dynein is an AAA+ motor responsible for intracellular cargo transport and force generation along microtubules (MTs). Unlike kinesin and myosin, dynein contains multiple ATPase subunits, with AAA1 serving as the primary catalytic site. ATPase activity at AAA3 is also essential for robust motility, but its role in dynein's mechanochemical cycle remains unclear. Here, we introduced transient pauses in *Saccharomyces cerevisiae* dynein motility by using a slowly hydrolyzing ATP analog. Analysis of pausing behavior revealed that AAA3 hydrolyzes nucleotide an order of magnitude slower than AAA1 and the two sites do not coordinate. ATPase mutations to AAA3 abolish the ability of dynein to modulate MT release. Nucleotide hydrolysis at AAA3 lifts this "MT gate" to fast motility. These results suggest that AAA3 acts as a switch that repurposes cytoplasmic dynein for fast cargo transport and MT anchoring tasks in cells.

INTRODUCTION

Eukaryotic cells employ adenosine triphosphate (ATP)-driven molecular motors to transport intracellular cargoes along cytoskeletal tracks. A primary system for these processes is the MT transport network, in which plus- and minus-end directed transport are driven by kinesin and cytoplasmic dynein, respectively. While cells employ a variety of kinesins for specific tasks, they typically only have a single cytoplasmic dynein heavy chain (*DHC1*) gene, responsible for many diverse tasks. In interphase cells, dynein transports vesicles, membranous organelles, mRNA and viruses[1–3]. It also functions as an MT anchor required for proper positioning of intracellular structures such as nucleus, Golgi and centrosomes during mitosis[1,4]. Defects in these processes have been linked to motor neuron degeneration, lissencephaly, and Alzheimer's disease[1,5,6]. Cytoplasmic dynein forms a multiprotein

*Correspondence should be addressed to: yildiz@berkeley.edu.

AUTHOR CONTRIBUTIONS

M.A.D and A.Y. designed experiments, M.A.D. and C.A.C. performed single-molecule inhibition assays, M.A.D. and V. B. collected and performed single-molecule motility assays, M.A.D. performed bulk ATPase assays, F.B.C performed optical trapping assays and monomer release assays, M.A.D., C.A.C. and F.B.C analyzed the data, and M.A.D. and A.Y. wrote the manuscript.

complex with a multitude of light and intermediate light chains, which primarily bind to the tail domain[7–9]. Regulatory proteins such as Lis1, NudE and Nudel bind to the motor domain and alter dynein motility[6,10,11]. Binding of dynein to organelles and vesicles also requires the dynactin complex and cargo adaptor proteins[6,12,13].

Dynein is a member of the AAA+ (ATPases associated with various cellular activities) superfamily, and shares no common ancestor with kinesin and myosin[14]. At the core of the cytoplasmic dynein holoenzyme lies a homodimer of two ~500 kDa heavy chains, which contain the catalytic and mechanical elements required for motility[15,16]. The motor domain consists of a pseudo-hexameric ring, with six non-identical AAA domains (AAA1–AAA6). Between AAA4 and AAA5, there protrudes a 15 nm coiled-coil stalk, bearing a small globular MT-binding domain (MTBD) (Fig. 1a). The two rings are connected by an N-terminal linker and dimerized through the tail domain[17].

Conformational changes that drive motility arise from ATP hydrolysis-dependent conformational changes within the AAA+ ring[17,18]. Assigning roles to each AAA+ site is complicated by the fact that the sequence and structure of each site is unique in dynein. Only AAA1–4 can bind nucleotide, while AAA5 and AAA6 do not have the conserved Walker A and B motifs required for ATP binding and hydrolysis[14,19,20]. The kinetics of dynein stepping are coupled to ATP hydrolysis at AAA1, which is strictly required for dynein motility[8]. ATP binding at AAA1 induces linker undocking, also referred to as the “priming stroke”[21,22]. ATP binding at AAA1 also induces release from the MT, by initiating helix sliding within the coiled-coil of the stalk[18,23,24]. Upon ATP hydrolysis at AAA1, dynein re-binds to the MT and docks its linker via a force-generating “power stroke”[18,21,25].

The roles of the other AAA domains in dynein motility are not well understood. Mutations that abrogate ATP binding or hydrolysis at AAA2 and AAA4 have a minimal effect on the velocity of dynein, instead only affecting the processivity[19,26]. In contrast, ATPase mutations at AAA3 reduce motor velocity and MT-stimulated ATPase by an order of magnitude[19,26] and show defects in AAA1-generated linker swing[22]. These mutants strongly localize to MTs *in vivo*[20] and slowly release from MTs in the presence of ATP *in vitro*[18]. The ATP binding and hydrolysis loops of AAA3 are conserved in cytoplasmic dyneins, but not in dyneins responsible for intraflagellar transport (IFT) or axonemal bending (Supplementary Fig. 1), suggesting that ATPase activity at AAA3 may be critical for repurposing cytoplasmic dynein for different cellular roles, which is not necessary for axonemal or IFT dyneins.

While these studies suggest that an intact AAA3 domain is required for robust motility[15,18,20,26], the precise role of the AAA3 site in dynein’s mechanochemical cycle remains unknown. One possibility is that the dynein stepping mechanism involves two coordinated nucleotide hydrolysis cycles at AAA1 and AAA3. This would require two ATP molecules to be hydrolyzed per step[27]. Another possibility is that each step requires a single ATP hydrolysis at AAA1[8], and AAA3 acts as a switch to turn allosteric communication within the ring on or off depending on its nucleotide state[1,15]. It also remained unclear why ATPase mutations to AAA3 slow down the catalytic activity and stepping rate of the motor

by an order of magnitude. These questions cannot be addressed through mutagenesis alone, because disrupting the ATPase activity of AAA3 also affects the ATPase of AAA1[15,18].

To define the role of AAA3 in dynein's mechanochemical cycle, we studied motility and catalytic activity of native and mutant dynein motors using optical trap, single-molecule fluorescence and bulk enzymology. We show that a functional AAA3 site is required for AAA1-dependent control of the MT attachment and detachment cycle. In AAA3 mutants, impaired release gates ATP hydrolysis at AAA1, and this gate is lifted with added salt. We analyzed coordination between the two sites by addition of the slowly-hydrolyzable ATP analog, ATPγS. ATPγS induced pauses in dynein motility, and the frequency of pausing increased with ATPγS concentration. Analysis of the pausing behavior revealed that ATPγS must bind to one site on each monomer to completely pause motility. In contrast to wild-type (WT) dynein, the motility of a dynein mutant unable to bind ATP at the AAA3 site was insensitive to ATPγS, indicating that pausing is initiated by ATPγS binding to the AAA3 sites only, and not to AAA1. A dynein construct with only one AAA3 site takes many successive fast steps between long pauses in the presence of equimolar ATP and ATPγS. These results showed that AAA3 does not hydrolyze ATP in concert with AAA1 during the mechanochemical cycle. Instead, when bound to a nucleotide in a post-hydrolysis state, it completes an allosteric circuit that allows AAA1 to modulate MT affinity. We propose that the AAA3 site acts as a "switch" that converts cytoplasmic dynein from transporting to anchoring modes of motility.

RESULTS

AAA3 mutants remain tightly-attached to MTs

ATPase mutations to dynein's AAA3 domain induce strong attachment to the MT and dramatically reduce motility[15,18,20,26]. Based on these results, we hypothesized that AAA3 is required for AAA1-directed MT release. To test this hypothesis, we characterized how mutations to the AAA3 site affect nucleotide-dependent release of dynein from MTs. Specifically, we expected monomeric dyneins bearing ATPase mutations to AAA3 to show no ATP-dependent increase in release rate from the MT, comparable to WT monomers in the absence of nucleotide.

We used point mutations to the Walker A (K–A mutation) and Walker B (E–Q mutation) motifs of the AAA1 and AAA3 sites[18,19] of an N-terminally truncated 331 kDa *S. cerevisiae* dynein monomer (referred to as $Dyn1_{331kD}$)[8]. To estimate the release rate of monomers from MTs, we labeled these motors with a tetramethylrhodamine (TMR) dye at the N-terminus and bound them to surface-immobilized MTs. Nucleotide-dependent MT affinities were measured by quantifying changes in total fluorescence signal for each MT after nucleotide addition[32] (Fig. 1b,c). Consistent with biochemical assays on *Dictyostelium* dynein[18], WT monomers did not release in the absence of nucleotide or in the presence of the non-hydrolyzable ATP analog, AMP-PNP. Upon addition of 2 mM ATP, a majority (60.5%) of WT monomers released from MTs. While $AAA1_{E–Q}$ (E1849Q) monomers released from MTs similarly (66%) to WT upon ATP addition, $AAA1_{K–A}$ (K1802A) showed minimal release, consistent with the previous finding that ATP binding, not hydrolysis, at AAA1 triggers MT release[14]. In comparison to WT, only ~20% of $AAA3_{K–A}$

and $AAA3_{E-Q}$ monomers released from MTs after ATP addition (Fig. 1c). These results showed that both ATP binding and hydrolysis mutations to AAA3 abolish nucleotide-dependent MT release of dynein, consistent with blocked communication from AAA1 to the MT.

To quantify the MT affinity of AAA3 mutants in comparison to WT, we measured the effect of applied force on the release rates of dynein monomers using optical trap[28]. Monomeric dyneins were attached to polystyrene beads from their C-termini using a short DNA tether. The motor-coated beads were moved ±125 nm between two positions above the MT in a square wave pattern[28]. Stochastic binding and release of dynein from MTs allowed measurement of release rate over a range of applied forces (1–12 pN) (Fig. 1d). In the absence of ATP (apo), individual WT monomers released from MTs with 7.7 s^{-1} pN^{-1} when force was applied towards the minus-end, while release towards the plus end was slower (0.04 s^{-1} pN^{-1})[28] (Fig. 1d and Supplementary Fig. 2). Addition of 1 mM ATP increased the release rate of WT monomers by an order of magnitude. In contrast, the MT release rates of $AAA3_{K-A}$ (K2424A) and $AAA3_{E-Q}$ (E2488Q) at 2 mM ATP (1.7 s^{-1} pN^{-1} and 0.04 s^{-1} pN^{-1} towards the MT minus-end and plus-end, respectively) were both similar to WT monomers in the apo state (Fig. 1e and Supplementary Fig. 2). Therefore, AAA3 mutants remain strongly attached to MTs in the presence of ATP and can only be removed from the MT by force, similar to WT in the apo state. Because ATP binding to AAA1 is required for MT release in WT dynein[18,23], our results suggest that communication from AAA1 to the MT requires a functional AAA3 domain.

AAA3 lifts an “MT gate” to robust motility

We next investigated the effects of alterations in MT affinity on the motility of a dynein dimer. The reduced motility and ATPase activity of AAA3 ATPase mutants may be related to the inability of AAA1 to control detachment from MTs without an active AAA3 site, such that impaired MT release slows down ATP hydrolysis at AAA1. Alternatively, AAA1 requires hydrolysis at AAA3 to proceed through its mechanochemical cycle. To distinguish between these possibilities, we reduced the MT affinity of dynein motors by increasing the salt (KCl) concentration, and measured the velocity and MT-stimulated ATPase rates of WT and AAA3 mutants. If MT detachment is rate-limiting in AAA3 mutants, we expected both the velocity and MT-stimulated ATPase activity to increase with added salt. If hydrolysis at AAA3 is required for the cycle to proceed, addition of salt was not expected to substantially affect motility.

To measure single-molecule velocity, we artificially dimerized $Dyn1_{331kD}$ monomers with a glutathione S-transferase (GST) tag. This construct has nearly identical motility properties to full-length dynein[8,9]. The velocity and run length of TMR-labeled motors along surface-immobilized axonemes were recorded at 0–200 mM KCl, using total internal reflection fluorescence (TIRF) microscopy (Fig. 2a,b,c). WT moved at 120 nm s^{-1} without added salt and its velocity remained largely unaffected with up to 100 mM added salt (Fig. 2d). In contrast, the velocity of $AAA3_{K-A}$ increased substantially with added salt. At 200 mM KCl, the velocity (42 nm s^{-1}) was 3 times greater compared to the no-salt condition (14 nm s^{-1})

(Fig. 2e). Run lengths for both WT and $AAA3_{K-A}$ decreased with added salt, consistent with reduced MT affinity (Supplementary Fig. 3).

To test whether increased MT release can speed up the AAA1 hydrolysis cycle in the absence of AAA3 activity, we measured the catalytic rate constant (k_{cat}) of WT and $AAA3_{K-A}$ at saturating MT concentrations and variable salt concentration. At 150 mM KCl, $k_{cat(MT)}$ of $AAA3_{K-A}$ increased by 70%, while $k_{cat(MT)}$ of WT decreased slightly (25%) (Fig. 2f,g). Addition of 100 mM salt increased the Michaelis-Menten constant (K_M) for MT by an order of magnitude for WT and $AAA3_{K-A}$, consistent with reduced MT affinity (Supplementary Table 1). We note that the velocity and ATP hydrolysis rate of $AAA3_{K-A}$ was lower than WT at high salt. Full recovery in speed and ATPase activity may require proper timing of strong and weak MT affinity states orchestrated with the force generation cycle, which cannot be achieved with salt titrations.

These results demonstrate why AAA3 mutants have dramatically reduced velocity and ATPase activity. ATP binding at AAA1 cannot direct release from the MT without an active AAA3 domain. In $AAA3_{K-A}$ mutants, MT release becomes rate-limiting and gates hydrolysis at AAA1, resulting in slow motility.

Single-molecule inhibition of dynein motility

We next turned our attention to the question of whether the AAA3 and AAA1 sites coordinate directly to drive MT release[27]. Alternately, AAA3 may serve as switch that allows AAA1 to communicate with the MTBD, and does not coordinate with AAA1[15,19,26] (Fig. 3a). Because mutations to the active site of AAA3 also affect the ATPase activity of AAA1, analysis of AAA1 and AAA3 mutants was not sufficient to address this question. We performed single-molecule enzyme inhibition experiments using a slowly-hydrolyzable ATP analog, ATPγS[29,30]. Binding of ATPγS, which mimics the ATP-bound state, to a motor stalled the nucleotide hydrolysis cycle and induced a pause in motility[31]. Analysis of pause frequency and duration provided insight into coordination among multiple ATPase sites[29,30,32,33]. To measure motility in the presence of ATPγS, WT dynein was labeled with a bright quantum dot (QD) and tracked at nanometer resolution for several minutes in the presence of saturating (1 mM) ATP and variable (0–100 μM) ATPγS[9]. In the absence of ATPγS, the motors moved at a nearly constant velocity of 120 nm s^{-1}. The addition of 2–100 μM ATPγS reduced the velocity of the motors (Supplementary Movie 1). Traces of individual motors revealed that slowing was due to transient pauses in motility (Fig. 3b). As the concentration of ATPγS increased, both the frequency and duration (Supplementary Fig. 4) of pausing increased.

The pause density (*PD*), defined as the number of pauses per unit length travelled by the motor, is related to the mole fraction of inhibitor-bound motors[29,32]. To calculate *PD*, we measured the residence time of individual motors within 50 nm bins along the MT axis (Supplementary Note, Fig. 3c). A residence time histogram fits well to a bi-exponential decay ($R^2 > 0.97$ for each [ATPγS] tested), revealing two distinct populations: “fast”, with a short residence time (0.374 ± 0.004 s, mean ± 95% confidence interval), and “slow”, with a long residence time (3.18 ± 0.45 s, Fig. 3d, Supplementary Fig. 4). The PD was calculated from the ratio of the slow population over the entire population (Supplementary Fig. 5).

To extract the binding parameters of ATPγS to dynein, *PD* as a function of ATPγS concentration was fit to a Hill equation (Fig. 3e), assuming that there were no intermediate states of the pausing behavior. The dissociation constant (K_d) of ATPγS for WT dynein was 9.9 ± 3.2 μM (mean ± s.d.), indicating that analog binding at the site of inhibition was nearly saturated by 100 μM. The Hill coefficient (n) was 1.97, indicating that two ATPγS must bind to the motor to initiate a pause[29,30,32]. The plot was not well-fit by fixing the Hill coefficient to $n = 1$ ($p = 0.03$, F-test).

The fit also revealed the maximum *PD* (PD_{MAX}, 0.011 nm^{-1}) at saturating ATPγS (Fig. 3e). Because the mean step size of dynein is ~8 nm, the result indicated that WT dynein takes ~11 steps between pauses at saturation. The velocity at saturation (36 nm s^{-1}, Supplementary Fig. 6) remained substantially faster than AAA3 and AAA1 mutant homodimers[19,26], indicating that the site of inhibition is not responsible for stepping[1,21–23]. To estimate the number of ATP hydrolysis events required for dynein stepping, we measured the velocity of WT at 200 nM – 1 mM ATP in the absence of ATPγS (Fig. 3f). Velocity measurements fitted well to Michaelis-Menten kinetics ($K_{M(ATP)}$ = 46.3 ± 6.5 μM (mean ± 95% c.i.), v_{max} = 114 nm s^{-1}), suggesting a single hydrolysis event per step. The results excluded a model with two coordinating ATP hydrolysis sites per step.

ATPγS specifically inhibits the AAA3 site

We next sought to identify which sites are inhibited by ATPγS. Because a single active head is sufficient to drive dynein motility[9] and two ATPγS are required to generate a pause (Fig. 3), we hypothesized that one ATPγS must bind to each head of the dimer during pauses. To test whether ATPγS preferentially binds to the AAA3 site to induce a pause, we measured the pausing behavior of the $AAA3_{K–A}$ mutant at saturating ATP and 0–1,000 μM ATPγS (Fig. 4a, Supplementary Movie 2). Surprisingly, we found that the velocity and *PD* of these mutants were entirely unaffected by ATPγS at all concentrations tested (Fig. 4b,c), indicating that the AAA1 site is insensitive to ATPγS. We conclude that ATPγS specifically inhibits AAA3 and both AAA3 sites in a dimer must be inhibited to initiate a pause.

We confirmed this result in bulk using ATPase assays at saturating MTs and varying concentrations of ATP (Fig. 4d,e and Supplementary Table 2). We measured the $K_{M(ATP)}$ and $k_{cat(ATP)}$ of WT and $AAA3_{K–A}$ in response to 0–40 μM (for WT) or 0–1,000 μM (for $AAA3_{K–A}$) ATPγS (Supplementary Note). Consistent with the velocity measurements (Fig. 3f), $K_{M(ATP)}$ for WT was 46 ± 5 μM in the absence of ATPγS and increased to 818 ± 80 μM at 10 μM ATPγS, while $k_{cat(ATP)}$ remained largely unaffected (17.0 ± 0.5 s^{-1} vs. 19.0 ± 0.7 s^{-1}, Supplementary Table 2), consistent with competitive inhibition. By comparison, the $AAA3_{K–A}$ homodimer was largely insensitive to ATPγS at concentrations of up to 1 mM, except for a modest increase in $K_{M(ATP)}$ from 38 ± 3 μM to 106 ± 36 μM. These results showed that ATPγS is a strong inhibitor of the AAA3 site, and not AAA1.

To gain insight into the mechanism of AAA3-specific inhibition, we measured the ATPγS hydrolysis rate of WT and $AAA3_{K–A}$ in the absence of ATP (Fig. 4f). $k_{cat(ATP\gamma S)}$ (2.3 ± 0.2 s^{-1} for $AAA3_{K–A}$ and 4.5 ± 0.4 s^{-1} for WT dynein) was relatively fast. $K_{M(ATP\gamma S)}$ was similar for WT and $AAA3_{K–A}$ (500 ± 110 μM for WT, 425 ± 98 μM for $AAA3_{K–A}$). These results indicated that the fast hydrolysis of ATPγS at high concentrations does not arise from

AAA3. This is because $k_{cat(ATP\gamma S)}$ was much faster than the pausing rate of WT in the presence of ATPγS ($k_{pause} = \tau_{pause}^{-1}$ = ~0.067 s, Supplementary Fig. 5c) and $K_{M(ATP\gamma S)}$ was much higher than $K_{M(ATP)}$ = 46.2 μM and K_D = 9.9 ± 1.6 μM measured from ATPase and *PD* analysis of WT, respectively (Fig. 3c). Instead, the remaining catalytic sites on dynein rapidly hydrolyze ATPγS, but display weak affinity, while the AAA3 site is de-activated in both constructs (by either mutagenesis or a tightly-bound ATPγS). We excluded that the results are not due to residual ATP contamination using ^{32}P nuclear magnetic resonance (NMR) spectroscopy (Supplementary Fig. 6).

AAA3 and AAA1 do not coordinate their hydrolysis cycles

Our observation that ATPγS specifically inhibits AAA3, but not AAA1 (Fig. 4), provided a unique opportunity to investigate the role of AAA3 in dynein's mechanochemical cycle. However, interpretation of WT homodimer motility in the presence of ATPγS is problematic because it contains two AAA3 sites and may have 0, 1 or 2 ATPγS bound with each state having a distinct velocity distribution. In fact, the velocity distribution of WT at low ATPγS concentrations showed signs of more than two subpopulations (Supplementary Fig. 5).

A dynein motor with a single active AAA3 site would be expected to switch between two states: a "fast", uninhibited state, and a "slow" inhibited state. For this purpose, we used a heterodimer of a WT monomer and a chimeric protein containing a seryl tRNA synthetase (SRS) domain fused to a dynein stalk-MTBD[23,34] (referred to as SRS-WT, Fig. 5a). SRS-WT moves processively at 35% of the speed of the WT homodimer[28]. Because SRS-WT contains a single AAA+ ring, we expected it to switch between fast and slow states without an intermediate in the presence of ATPγS. We tracked the motility of QD-labeled SRS-WT at 1 mM ATP and 0–100 μM ATPγS. As the ATPγS concentration was increased, the velocity of SRS-WT decreased due to frequent pauses (Fig. 5a), similar to WT (Fig. 3a). Normalized histograms of motor velocity revealed two distinct populations (Fig. 5b). The velocity of the fast state was 68 ± 31 nm s^{-1}, whereas the motor was nearly immotile (−1.2 ± 8.2 nm s^{-1}, mean ± s.d.) in the slow state (Fig. 5b). We observed a shift from the fast to the slow population as the ATPγS concentration increased. Overlaid velocity histograms at different ATPγS intersected in a single point (Fig. 5b), consistent with two-state inhibition of SRS-WT by ATPγS.

PD was calculated from residence times in 50 nm bins (Supplementary Note, Supplementary Fig. 7) and was fitted to a Hill equation with n = 1 (Fig. 5c), consistent with two-state inhibition. K_D was similar to WT (7.8 ± 2.4 μM vs. 9.9 ± 1.6 μM, mean ± 95% confidence interval), and pausing was saturated at 100 μM ATPγS. Unlike WT (Supplementary Fig. 5), the pause duration remains nearly constant (~15 s) at all ATPγS concentrations tested (Fig. 5d), suggesting that exit from a pause is limited by release of a single bound ATPγS, and consecutive pauses are separated by long runs of fast motility.

If AAA3 hydrolyzes an ATP at every step of the motor, we expected the motor to pause after taking each step at saturating ATPγS[9,30]. If the AAA3 instead acts as a switch with a slower hydrolysis cycle than AAA1, we expect SRS-WT to take many fast steps between pauses, because a persistently bound hydrolysis product at AAA3 would prevent re-

inhibition (Fig 3a). The PD_{MAX} for SRS-WT was 0.0063 pause nm^{-1} (Fig. 5c), indicating that SRS-WT embarks on fast runs for many steps between long-lived pausing events.

The presence of extended fast runs between pauses was also apparent from traces of SRS-WT at saturating ATPγS (100 μM) and ATP (1 mM) (Fig. 6a). However, long runs of fast motility between pauses could also result from the high (10:1) ATP:ATPγS ratio used in these assays[18,19,26]. To exclude this possibility, we analyzed the pausing behavior of SRS-WT at 2:1 (200 μM ATP, 100 μM ATPγS, Fig. 6b) and 1:1 (100 μM ATP, 100 μM ATPγS, Fig. 6c) ATP:ATPγS. Compared to 10:1 ATP:ATPγS conditions, the overall velocity of the motors was reduced only 50% (Fig. 6d), due to the reduction in the frequency of fast runs (0.03 and 0.02 s^{-1} for 2:1 and 1:1, respectively) (Fig. 6e). Traces of single motors still exhibited fast runs extend over 15 steps on average at 1:1 ATP:ATPγS (Fig. 6f), demonstrating that the presence of fast runs between pauses was not due to the high ATP:ATPγS ratio. Instead, when AAA3 binds and hydrolyzes ATP, the hydrolysis products remain bound for a long period of time, allowing the motor to take many steps before AAA3 can be re-inhibited by ATPγS.

DISCUSSION

Our results illuminate the role of the AAA3 site in the cytoplasmic dynein mechanochemical cycle. We found that ATPase mutations to AAA3 disrupt ATP-induced release of dynein from MT, indicating that the AAA3 domain is essential for communication between AAA1 and the MTBD. Using single-molecule enzyme inhibition assays, we find that ATPγS specifically inhibits AAA3, granting a unique opportunity to investigate this site in further detail. We found that AAA1 and AAA3 do not coordinate directly. Instead, AAA3 hydrolyzes ATP an order of magnitude slower than AAA1 and is decoupled from the mechanochemical cycle.

Combining these results with previous work, we propose that AAA3 acts as a switch that regulates AAA1-directed MT release (Fig. 7). In the apo or ATP-bound state (mimicked by AAA3 ATP-binding and hydrolysis mutants, respectively), AAA1 cannot allosterically direct MT release through the ring (Fig. 7, **Left**)[15,19,26]. In this switch off state, dynein remains processive, albeit at a substantially lower speed[26], presumably via tension generated on the MTBD through the powerstroke of the linker[17,28] (Fig. 1e,f). Slow MT detachment in turn slows the hydrolysis cycle at AAA1, resulting in reduced speed and strong MT attachment. After ATP hydrolysis at AAA3, the switch is on, and the allosteric circuit connects AAA1 to MTBD, allowing rapid, ATP-stimulated release from the MT (Fig. 7, **right**). This “switch on” post-hydrolysis state (either ADP-P_i or ADP) persists for an average of ~20 steps of the motor, allowing the motors to move at full speed. Conformational changes required for release from the MT is driven by ATP hydrolysis in AAA1[18,23]. Eventual release of products at AAA3 turns the switch off until the next nucleotide cycle.

A possible clue for the molecular basis of the AAA3 switch comes from structural studies of dynein and other AAA motors, in which allosteric communication across the ring is driven by coupled rigid-body motions of the subunits[15,16,35–38]. In dynein, these motions initiate

with ATP binding to AAA1[16,36]. The ATP binding cleft at the AAA1 site has an open conformation in the apo state, consistent with its low affinity for ATPγS (Fig. 4f). ATP binding induces AAA1–AAA2 gap closure[15,16,36], leading to rigid-body rearrangement of AAA2–4[15,35,36,38]. These rearrangements in the AAA+ ring may create an allosteric circuit that connects AAA1 to the base of the stalk to couple ATP hydrolysis with control of MT binding affinity[15,23,34]. Our results indicate that AAA3 plays a major regulatory role in this circuit. In the apo or ATP-bound states of AAA3, the communication between AAA1 and the base of stalk is disrupted. In a post-hydrolysis state of AAA3, AAA1 can efficiently direct AAA3 rearrangement, which in turn couples to MT release through AAA4/5[1,15,16].

Our model has implications for the role of AAA3 in dynein's cellular functions. We showed that dynein switches between fast and slow motility based upon the nucleotide state of AAA3. We speculate that regulation of AAA3 within cells can repurpose cytoplasmic dynein for different tasks, e.g. from rapidly transporting intracellular cargos along the length of an MT to anchoring of astral MTs to the cell cortex during mitosis[6,39]. Because the cellular concentration of ATP is saturating for dynein, the AAA3 switch is expected to be "on" for the majority of the time. The AAA3 switch may be allosterically regulated by adaptor proteins that bind to the dynein motor domain. One clue comes from studies of the dynein regulatory protein Lis1, which binds to the AAA+ ring near AAA3[11,40]. The LIS1-dynein complex also shows persistent MT attachment and bears a strong resemblance in its velocity to AAA3 mutants[11,40]. Interestingly, a similar phenotype can also be recapitulated by mutating the sensor arginine of AAA4 that reaches into the AAA3 ATP binding pocket[40]. Further work on conformational changes within the AAA+ ring as a function of the nucleotide state of AAA3 and how dynein-associated proteins affect these conformational states is required to elucidate the regulation of the dynein motor domain[11,40–42].

ONLINE METHODS

Cloning and molecular biology

We used an N-terminal truncated *S. cerevisiae* cytoplasmic dynein gene (*DYN1*) truncated at the N terminus (encoding amino acids 1219–4093) and artificially dimerized through an N-terminal GST tag (referred to as GST-Dyn1$_{331kD}$) as a template for mutagenesis[8]. Dynein constructs were tagged with HaloTag (Promega) either at the N or C terminus for fluorescent labeling[8,9]. K1694A mutation was inserted into GFP-GST-Dyn1$_{331kD}$ by homologous recombination. To construct the SRS-WT heterodimer, a monomeric dynein bearing an N-terminal FRB domain (FRB-Dyn1$_{331kD}$-Halo)[8] was dimerized with a chimeric construct, which consists of SRS fused with a dynein stalk-MTBD and a C-terminal FKBP12 tag. The stalk registry (85:82) of the SRS construct ensures tight binding of the MTBD to MTs[23,34]. Heterodimers were constructed by mixing 1 μL of 500 nM FRB-Dyn1$_{331kD}$ with 1 μL of 5 μM FKBP12-SRS$_{85:82}$, 2 μL of 600 nM rapamycin[43,44].

Protein expression, purification and labeling

Dynein proteins were expressed in yeast and affinity purified as described[8]. Active motors were purified by the MT bind-and-release assay[8,9,45] and stored in dynein loading buffer

(DLB: 30 mM HEPES pH 7.2, 2 mM $MgCl_2$, 1 mM EGTA, 10% glycerol). Expression and purification of SRS-MTBD was carried out from *E.coli*, as described[34]. For velocity measurements, the motors were labeled with 10 μM TMR HaloTag ligand for 1 h on ice during protein preparation, prior to washing of the Immunoglobulin G beads. For high resolution tracking measurements of WT dynein, amine-modified QDs emitting at 655 nm (QD655, Life Technologies) were coated with a HaloTag ligand and incubated with dynein motors for 10 minutes on ice before the single-molecule assays[9]. For WT dynein, 1 μL of 500 nM dynein was labeled with 1 μL 2 μM QD655 for 10 minutes. To label the $AAA3_{K-A}$ mutant, carboxy-coated QD655 was coated with anti-GFP polyclonal antibody (COVQ21936, Covance) using EDC crosslinking. Binding of GFP to antibody was specific, because QDs that are not coated with antibody did not label the motor (not shown). 1 μL of 1 μM anti-GFP antibody-coated QD655 was mixed with 1 μL ~500 nM $AAA3_{K-A}$ mutant dynein, containing an N-terminal GFP.

Microscope and imaging

Single-molecule motility assays were performed on a custom-built objective-type total internal reflection fluorescence (TIRF) microscope, equipped with an inverted microscope body (Nikon Ti-Eclipse) with perfect focusing system, 1.45 NA 60× microscope objective (Nikon, TIRF Plan Apochromat). The sample was illuminated with 488 nm and 532 nm laser beams (Coherent) to image QDs and TMR, respectively. Movies of TMR-labeled dynein were recorded with a 0.5 – 2.0 s exposure time under ~2 mW 532 nm excitation. QD655-labeled dyneins were imaged with a 50–100 ms exposure time. Fluorescence signal was detected with an ORCA-Flash4.0 sCMOS camera (Hamamatsu).

Single-molecule motility assays

Motility assays were performed in hand-made flow chambers[8,45]. Sea urchin axonemes were immobilized on a glass coverslip in a flow camber constructed with double-sided tape. The chamber was washed with 15 μl of DLB, followed by 15 μl of DLBC (DLB supplemented with 1 mg ml^{-1} casein, 2 mM dithiothreitol (DTT)). 100–500 pM dynein was then perfused into the chamber in DLBC and allowed to bind to the axonemes for 1 minute. The flow cell was then washed with 45 μl DLBC (three 15 μl washes) followed by 20 μl of imaging buffer carrying the appropriate salt and nucleotide condition.

For velocity measurements, TMR-labeled dyneins were imaged in the presence of DLBC at 1 mM ATP, supplemented with 0–200 mM KCl, 25 mM Protocatechuic Acid (PCA) and 0.35 mg ml^{-1} Protocatechuate Dioxygenase (PCD) for oxygen scavenging[46], 0.6 mM Trolox for triplet state quenching[47], 2 mM phosphoenolpyruvate and 0.1 mg ml^{-1} pyruvate kinase to regenerate ATP in the chamber. When working at ATP concentrations below 5 μM, we corrected for stage drift by tracking immobilized deep-red fiducial beads on the slide concurrently with data acquisition and subtracting their velocities from the measured velocities of dynein molecules. To measure the pausing behavior, QD-labeled dynein motors were imaged in an imaging buffer consisting of DLBC at 100–1000 μM ATP, and 0–1000 μM ATPγS, supplemented with 10 mM β-mercaptoethanol to prevent blinking[48], 2 mM phosphoenolpyruvate and 0.1 mg ml^{-1} pyruvate kinase (SigmaAldrich) to regenerate ATP.

Dynein MT-release under ATP flow

Sea urchin axonemes were immobilized on a glass coverlsip in a flow chamber, which allows buffer exchange while the chamber was mounted to the microscope stage. Axonemes were decorated with 20 μl of ~15 nM monomeric TMR-labeled dynein in DLBC without ATP and washed twice with DLBC to remove excess motor. The sample was then washed with imaging buffer, which does not contain ATP, and TMR fluorescence was monitored under TIRF illumination. MT-bound dynein motors were monitored for 100 frames at 280 ms temporal resolution before exchanging the assay solution with imaging buffer plus nucleotide. The percentage of released dynein monomers was quantified by taking the average TMR fluorescence intensity along 5 MTs per movie (3 movies per nucleotide condition) for 10 s before and after flow, and by subtracting the background intensity from TMR fluorescence. The change in intensity before and after flow was normalized by the intensity before flow. The reduction of fluorescence intensity was not due to permanent photobleaching of TMR, which is minimal on the timescale of our experimental conditions, as confirmed by repeating the flow experiment in the absence of nucleotide.

Optical trap assays

Optical trapping assays were performed using a custom-built optical trap, as described previously[28]. To apply forces through the C-terminal ring domain, dynein monomers with a C-terminal Halo-tag were labeled with a short (74 bp) double-stranded DNA strand containing biotin at its distal end. The dynein-DNA-biotin complex was incubated with streptavidin-coated polystyrene beads (0.86 μm diameter, Invitrogen). The motor-bead mixture was then diluted to 10% in DLBC supplemented with 5 mg ml^{-1} casein, the PCA and PCD oxygen scavenging system and 2 mM ATP. For the apo condition, ATP was not added the motor bead-mixture, resulting in residual ATP concentrations of ~40 nM, three orders of magnitude below dynein's $K_{M(ATP)}$ of ~26 μM[29]. The final bead concentration was 0.1% weight by volume. Cy5-labeled axonemes were adsorbed to the surface of a flow cell prior to addition of the bead and dynein mixture. The beads were trapped by a ~50 mW 1064 nm laser beam (Compass 1064, Coherent) to achieve a spring constant of ~0.05 pN nm^{-1}. Trapped beads were positioned over a Cy5-labeled axoneme and oscillated between two positions (±125 nm) along the long axis of the axoneme. Microtubule polarity was determined by imaging GFP-labeled kinesin motors, which decorate the plus-end of MTs. Motors were diluted until we observed 5–15% binding probability during the oscillation of the beads. >90% of the binding events terminated with a single release step, indicative of binding of a single dynein monomer.

ATPase assays

MTs were prepared using standard techniques. Briefly, 3.5 mg ml^{-1} purified bovine tubulin in BRB80 buffer (80 mM PIPES pH 6.8, 1mM $MgCl_2$, 1 mM EGTA) was polymerized by addition of 1 mM GTP, followed by stepwise addition of 10% volume each of 4 μM, 40 μM, and 400 μM paclitaxel at 5 minute intervals. MTs were pelleted at >50,000 × g and resuspended in DLB prior to use in ATPase assays.

The ATPase assays were carried out using EnzCheck Phosphate Assay Kit (Life Technologies). Dynein concentration was determined using absorbance of EGFP and ε_{GFP} =

55,000 cm^{-1} M^{-1} at 495 nm. A typical assay reaction consisted of DLB with 2–5 nM dynein, 200 nM methylthioguanosine, 1 U ml^{-1} purine nucleoside phosphorylase, 2 mM DTT, taxol-stabilized MTs, and ATP, ATPγS, and 0–200 mM KCl. Total reaction volume was 100–150 μL per sample. Rates of P_i generation were measured using a 96-well plate reader (μQuant, BioTek Instruments) set to record A360 at 60 second intervals against a buffer-only blank.

NMR

NMR spectra of 1 mM ATP, ADP, ATPγS, and ATP+ATPγS in D_20 were collected with a 300 MHz DD2 spectrometer (Agilent) using a 5 mm probe. Spectra were acquired and averaged over 6–24 hours. For the ATPγS and ATP+ATPγS spectra, shifts were assigned using the β-phosphate triplet at −24.01 ppm as a reference[49].

Supplementary Material

Refer to Web version on PubMed Central for supplementary material.

ACKNOWLEDGEMENTS

We are grateful to S. Can and J. Bandaria for critical reading of this manuscript, and C. Slack and A. Truxal for help with NMR spectroscopy. This work was supported by US National Institute of Health (GM094522 (AY)), US National Science Foundation CAREER Award (MCB-1055017 (AY)) and Graduate Research Fellowship (DGE 1106400 (FBC)), and Burroughs Wellcome Foundation (AY).

REFERENCES

1. Roberts AJ, Kon T, Knight PJ, Sutoh K, Burgess SA. Functions and mechanics of dynein motor proteins. Nat. Rev. Mol. Cell Biol. 2013; 14:713–726. [PubMed: 24064538]
2. Hendricks AG, Holzbaur ELF, Goldman YE. Force measurements on cargoes in living cells reveal collective dynamics of microtubule motors. Proc. Natl. Acad. Sci. U. S. A. 2012; 2012:1–6.
3. Dixit R, Ross JL, Goldman YE, Holzbaur ELF. Differential regulation of dynein and kinesin motor proteins by tau. Science. 2008; 319:1086–1089. [PubMed: 18202255]
4. Laan L, et al. Cortical dynein controls microtubule dynamics to generate pulling forces that position microtubule asters. Cell. 2012; 148:502–514. [PubMed: 22304918]
5. Stokin GB, Goldstein LSB. Axonal transport and Alzheimer's disease. Annu. Rev. Biochem. 2006; 75:607–627. [PubMed: 16756504]
6. Kardon JR, Vale RD. Regulators of the cytoplasmic dynein motor. Nat Rev Mol Cell Biol. 2009; 10:854–865. [PubMed: 19935668]
7. Gennerich A, Carter AP, Reck-Peterson SL, Vale RD. Force-induced bidirectional stepping of cytoplasmic dynein. Cell. 2007; 131:952–965. [PubMed: 18045537]
8. Reck-Peterson SL, et al. Single-molecule analysis of dynein processivity and stepping behavior. Cell. 2006; 126:335–348. [PubMed: 16873064]
9. DeWitt MA, Chang AY, Combs PA, Yildiz A. Cytoplasmic dynein moves through uncoordinated stepping of the AAA+ ring domains. Science. 2012; 335:221–225. [PubMed: 22157083]
10. Vallee RB, McKenney RJ, Ori-McKenney KM. Multiple modes of cytoplasmic dynein regulation. Nat Cell Biol. 2012; 14:224–230. [PubMed: 22373868]
11. McKenney RJ, Vershinin M, Kunwar A, Vallee RB, Gross SP. LIS1 and NudE induce a persistent dynein force-producing state. Cell. 2010; 141:304–314. [PubMed: 20403325]
12. McKenney RJ, Huynh W, Tanenbaum ME, Bhabha G, Vale RD. Activation of cytoplasmic dynein motility by dynactin-cargo adapter complexes. Science (80-.). 2014; 345:337–341.

13. Schlager MA, Hoang HT, Urnavicius L, Bullock SL, Carter AP. In vitro reconstitution of a highly processive recombinant human dynein complex. EMBO J. 2014
14. Mocz G, Gibbons IR. Model for the motor component of dynein heavy chain based on homology to the AAA family of oligomeric ATPases. Structure. 2001; 9:93–103. [PubMed: 11250194]
15. Kon T, et al. The 2.8 A crystal structure of the dynein motor domain. Nature. 2012; 484:345–350. [PubMed: 22398446]
16. Schmidt H, Gleave ES, Carter AP. Insights into dynein motor domain function from a 3.3-A crystal structure. Nat Struct Mol Biol. 2012
17. Burgess SA, Walker ML, Sakakibara H, Knight PJ, Oiwa K. Dynein structure and power stroke. Nature. 2003; 421:715–718. [PubMed: 12610617]
18. Imamula K, Kon T, Ohkura R, Sutoh K. The coordination of cyclic microtubule association/dissociation and tail swing of cytoplasmic dynein. Proc Natl Acad Sci U S A. 2007; 104:16134–16139. [PubMed: 17911268]
19. Kon T, Nishiura M, Ohkura R, Toyoshima YY, Sutoh K. Distinct functions of nucleotide-binding/hydrolysis sites in the four AAA modules of cytoplasmic dynein. Biochemistry. 2004; 43:11266–11274. [PubMed: 15366936]
20. Silvanovich A, Li M-G, Serr M, Mische S, Hays TS. The third P-loop domain in cytoplasmic dynein heavy chain is essential for dynein motor function and ATP-sensitive microtubule binding. Mol. Biol. Cell. 2003; 14:1355–1365. [PubMed: 12686593]
21. Roberts AJ, et al. AAA+ Ring and linker swing mechanism in the dynein motor. Cell. 2009; 136:485–495. [PubMed: 19203583]
22. Kon T, Mogami T, Ohkura R, Nishiura M, Sutoh K. ATP hydrolysis cycle-dependent tail motions in cytoplasmic dynein. Nat Struct Mol Biol. 2005; 12:513–519. [PubMed: 15880123]
23. Kon T, et al. Helix sliding in the stalk coiled coil of dynein couples ATPase and microtubule binding. Nat. Struct. Mol. Biol. 2009; 16:325–333. [PubMed: 19198589]
24. Carter AP, et al. Structure and functional role of dynein's microtubule-binding domain. Science (80-.). 2008; 322:1691–1695.
25. Roberts AJ, et al. ATP-driven remodeling of the linker domain in the dynein motor. Structure. 2012; 20:1670–1680. [PubMed: 22863569]
26. Cho C, Reck-Peterson SL, Vale RD. Regulatory ATPase sites of cytoplasmic dynein affect processivity and force generation. J Biol Chem. 2008; 283:25839–25845. [PubMed: 18650442]
27. Ross JL, Wallace K, Shuman H, Goldman YE, Holzbaur EL. Processive bidirectional motion of dynein-dynactin complexes in vitro. Nat Cell Biol. 2006; 8:562–570. [PubMed: 16715075]
28. Cleary FB, et al. Tension on the linker gates the ATP-dependent release of dynein from microtubules. Nat. Commun. 2014; 5:4587. [PubMed: 25109325]
29. Chemla YR, et al. Mechanism of force generation of a viral DNA packaging motor. Cell. 2005; 122:683–692. [PubMed: 16143101]
30. Sen M, et al. The ClpXP Protease Unfolds Substrates Using a Constant Rate of Pulling but Different Gears. Cell. 2013; 155:636–646. [PubMed: 24243020]
31. Guydosh NR, Block SM. Backsteps induced by nucleotide analogs suggest the front head of kinesin is gated by strain. Proc Natl Acad Sci U S A. 2006; 103:8054–8059. [PubMed: 16698928]
32. Moffitt JR, et al. Intersubunit coordination in a homomeric ring ATPase. Nature. 2009; 457:446–450. [PubMed: 19129763]
33. Chistol G, et al. High degree of coordination and division of labor among subunits in a homomeric ring ATPase. Cell. 2012; 151:1017–1028. [PubMed: 23178121]
34. Gibbons IR, et al. The affinity of the dynein microtubule-binding domain is modulated by the conformation of its coiled-coil stalk. J Biol Chem. 2005; 280:23960–23965. [PubMed: 15826937]
35. Glynn SE, Martin A, Nager AR, Baker TA, Sauer RT. Structures of asymmetric ClpX hexamers reveal nucleotide-dependent motions in a AAA+ protein-unfolding machine. Cell. 2009; 139:744–756. [PubMed: 19914167]
36. Carter AP, Cho C, Jin L, Vale RD. Crystal structure of the dynein motor domain. Science (80-.). 2011; 331:1159–1165.

37. Zhang X, et al. Structure of the AAA ATPase p97. Mol. Cell. 2000; 6:1473–1484. [PubMed: 11163219]
38. Lee S, et al. The structure of ClpB: a molecular chaperone that rescues proteins from an aggregated state. Cell. 2003; 115:229–240. [PubMed: 14567920]
39. Yi JY, et al. High-resolution imaging reveals indirect coordination of opposite motors and a role for LIS1 in high-load axonal transport. J. Cell Biol. 2011; 195:193–201. [PubMed: 22006948]
40. Huang J, Roberts AJ, Leschziner AE, Reck-Peterson SL. Lis1 Acts as a “Clutch” between the ATPase and Microtubule-Binding Domains of the Dynein Motor. Cell. 2012; 150:975–986. [PubMed: 22939623]
41. Markus SM, Kalutkiewicz Ka, Lee W-L. She1-mediated inhibition of dynein motility along astral microtubules promotes polarized spindle movements. Curr. Biol. 2012; 22:2221–2230. [PubMed: 23142046]
42. Firestone AJ, et al. Small-molecule inhibitors of the AAA+ ATPase motor cytoplasmic dynein. Nature. 2012; 484:125–129. [PubMed: 22425997]
43. Banaszynski LA, Liu CW, Wandless TJ. Characterization of the FKBP. rapamycin. FRB ternary complex. J Am Chem Soc. 2005; 127:4715–4721. [PubMed: 15796538]
44. Kliegman JI, et al. Chemical Genetics of Rapamycin-Insensitive TORC2 in S. cerevisiae. Cell Rep. 2013; 5:1725–1736. [PubMed: 24360963]
45. Yildiz A, Tomishige M, Vale RD, Selvin PR. Kinesin walks hand-over-hand. Science (80-.). 2004; 303:676–678.
46. Aitken CE, Marshall RA, Puglisi JD. An oxygen scavenging system for improvement of dye stability in single-molecule fluorescence experiments. Biophys J. 2008; 94:1826–1835. [PubMed: 17921203]
47. Rasnik I, McKinney SA, Ha T. Nonblinking and long-lasting single-molecule fluorescence imaging. Nat Methods. 2006; 3:891–893. [PubMed: 17013382]
48. Hohng S, Ha T. Near-complete suppression of quantum dot blinking in ambient conditions. J Am Chem Soc. 2004; 126:1324–1325. [PubMed: 14759174]
49. Kingsley-Hickman PB, et al. Phosphorus-31 NMR studies of ATP synthesis and hydrolysis kinetics in the intact myocardium. Biochemistry. 1987; 26:7501–7510. [PubMed: 3427090]

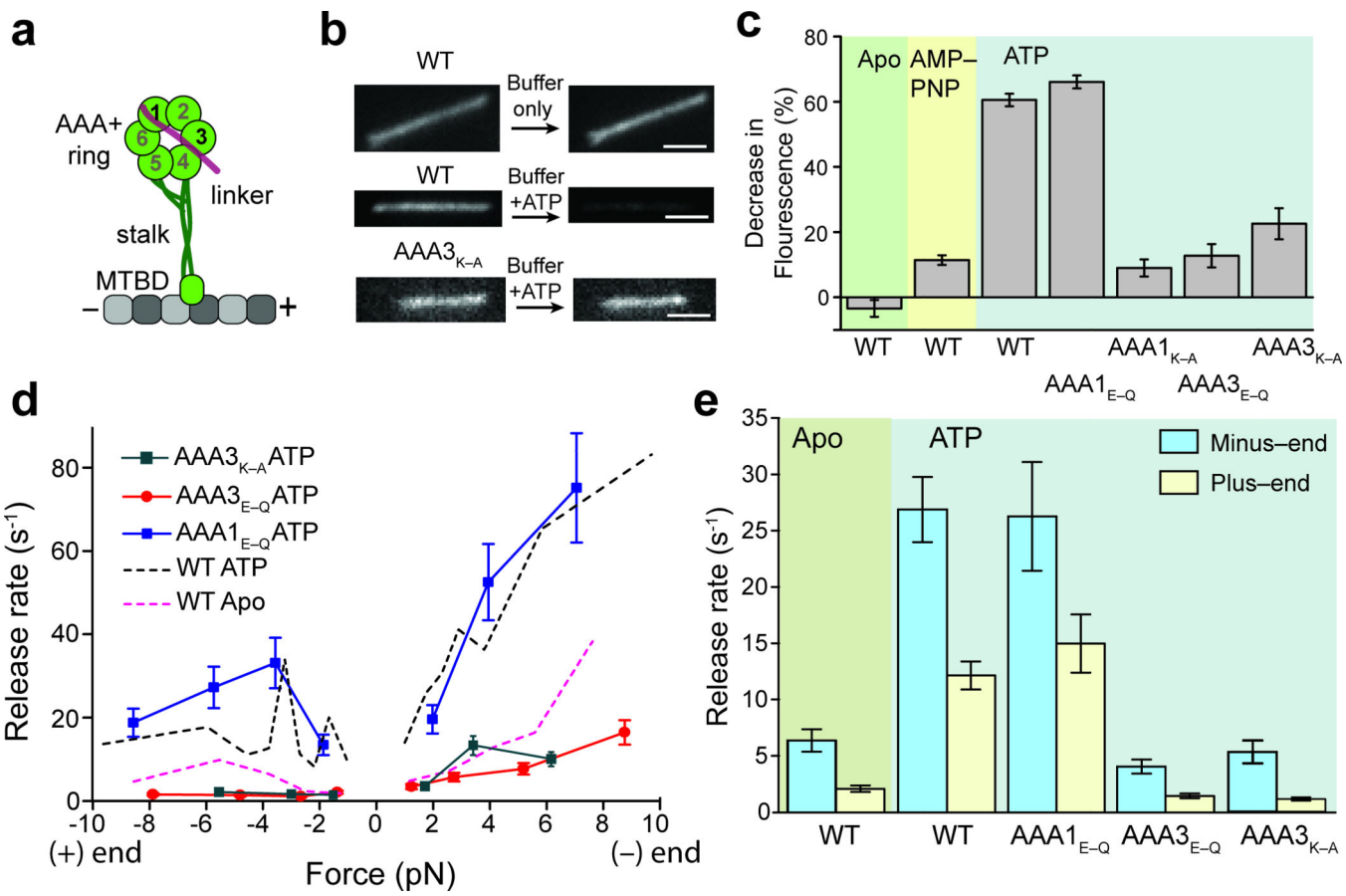

Figure 1. ATPase mutations to the AAA3 site abolish nucleotide-dependent release of dynein from MTs

(**a**) The dynein motor domain consists of a ring of six AAA+ sites (numbered in black). ATP hydrolysis at AAA1 and AAA3 are required for robust motility. (**b**) Images of MTs decorated with TMR-labeled dynein monomers were recorded before and after flow with the indicated solution. Scale bar is 2 μm. (**c**) The fraction of monomers released for different nucleotide treatments. Error bars represent s.e.m. of 15 MTs for each condition. (**d**) Force-dependent release rates of $AAA1_{E–Q}$ and $AAA3_{E–Q}$ mutants. MT release rates of the WT monomer in the presence and absence of ATP are shown for comparison. Error bars on each bin represent s.e.m. of 100 release events. (**e**) The average release rates of dynein mutants under 1–3 pN of load either toward the minus- or plus-end of MTs (n = 192 for the plus-end direction and 164 for the minus-end direction, ±95% confidence interval).

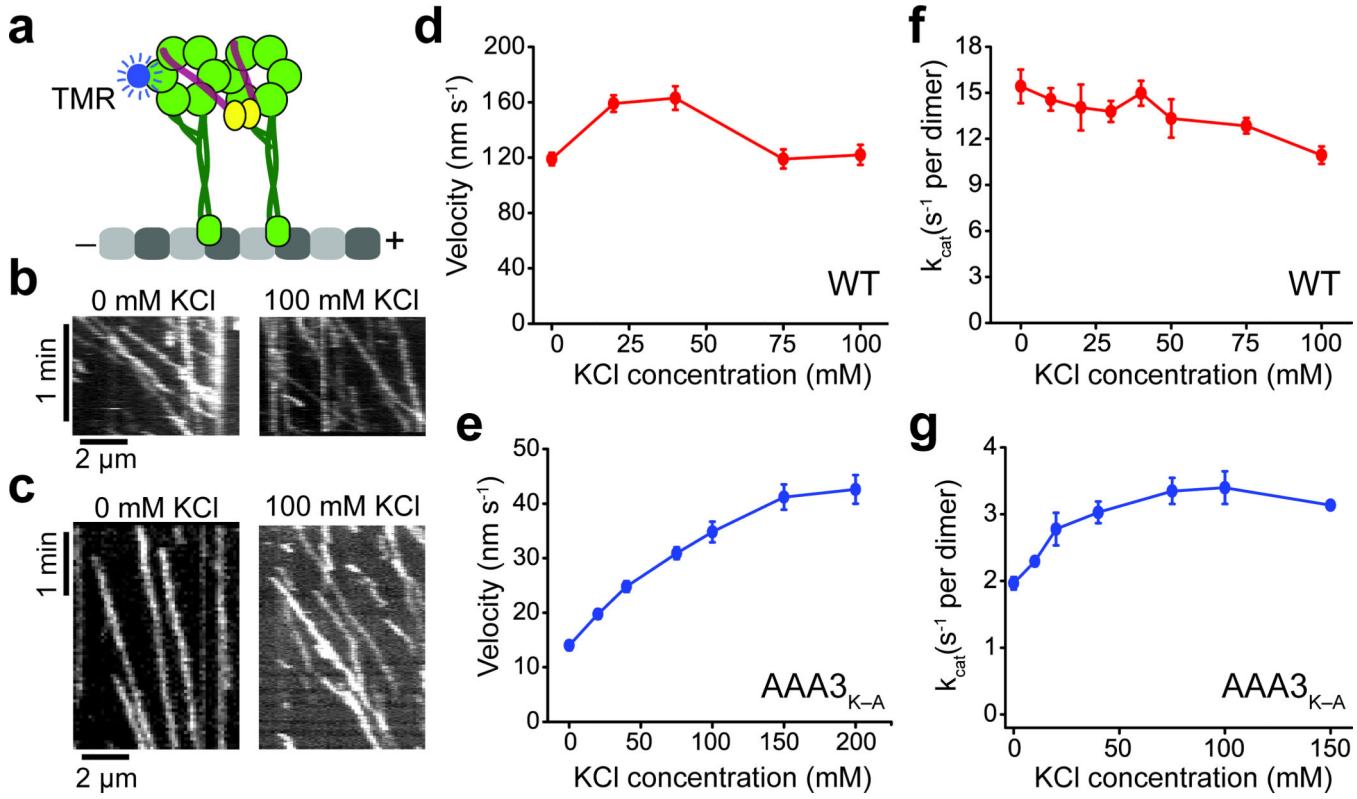

Figure 2. Dynein motility is gated by MT release in the absence of an active AAA3 site

(**a**) Schematic of $Dyn1_{331kD}$ dimerized through GST. (**b,c**) Kymographs of TMR-labeled WT (**b**) and $AAA3_{K–A}$ (**c**) walking along axonemes at 1 mM ATP. (**d,e**) Single-molecule velocities of WT (**d**) and $AAA3_{K–A}$ (**e**) at 1 mM ATP and 0–100 mM KCl. Error bars represent s.e.m. (n >88 for $AAA3_{K–A}$, n >126 for WT per concentration). (**f,g**) MT-stimulated ATPase activity of WT (**f**) and $AAA3_{K–A}$ (**g**) as a function of added KCl. Error bars represent s.e.m of 3 technical replicates.

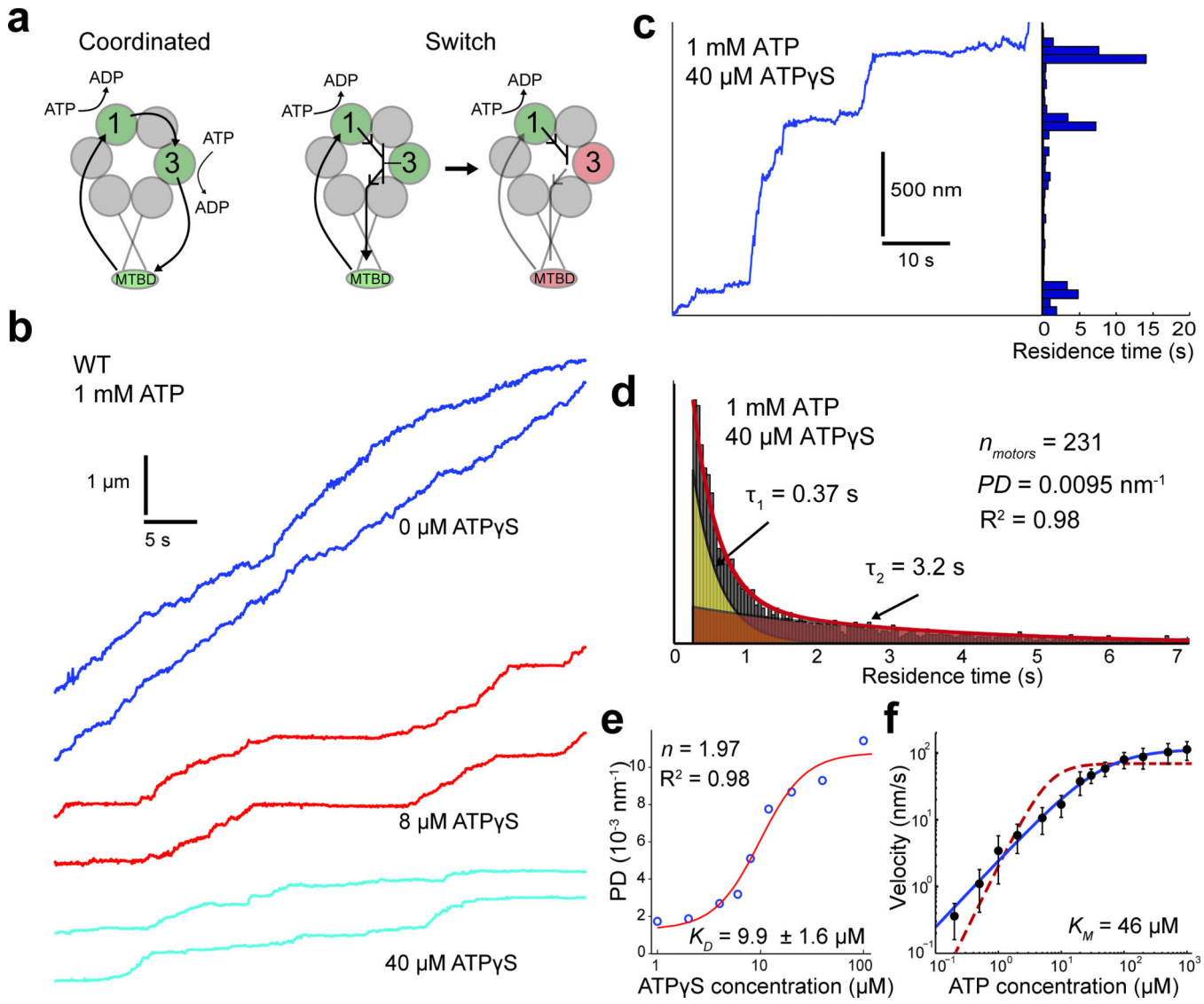

Figure 3. Single-molecule enzyme inhibition of dynein by ATPγS

(**a**) AAA3 may facilitate MT release either by directly coordinating its ATP hydrolysis cycle with that of AAA1 (left), or by controlling an allosteric "switch" that allows AAA1 to communicate with the MTBD (right). (**b**) Representative traces of WT dynein motility at 1 mM ATP and varying amounts of ATPγS (n = 120). The frequency of pauses increases at higher ATPγS concentrations. (**c**) The residence time histogram of a single motor for each 50 nm distance travelled along its path. Peaks indicate locations in which the motor experiences a prolonged pause. (**d**) The cumulative residence time histogram of 120 traces fits well to biexponential decay (red curve). The areas under the red and yellow curves represent the slow and fast populations, respectively. (**e**) *PD* (blue circles) as a function of ATPγS concentration. Red curves represents a fit to to the Hill equation. (**f**) Velocity of WT dynein as a function of ATP concentration (black circles) fits well (R^2 = 0.996) to Michaelis-Menten kinetics (blue curve) and deviates away (R^2 = 0.72) from Hill Equation with n = 2 (red dashed curve). Error bars represent s.d. of 120–246 traces of single motors.

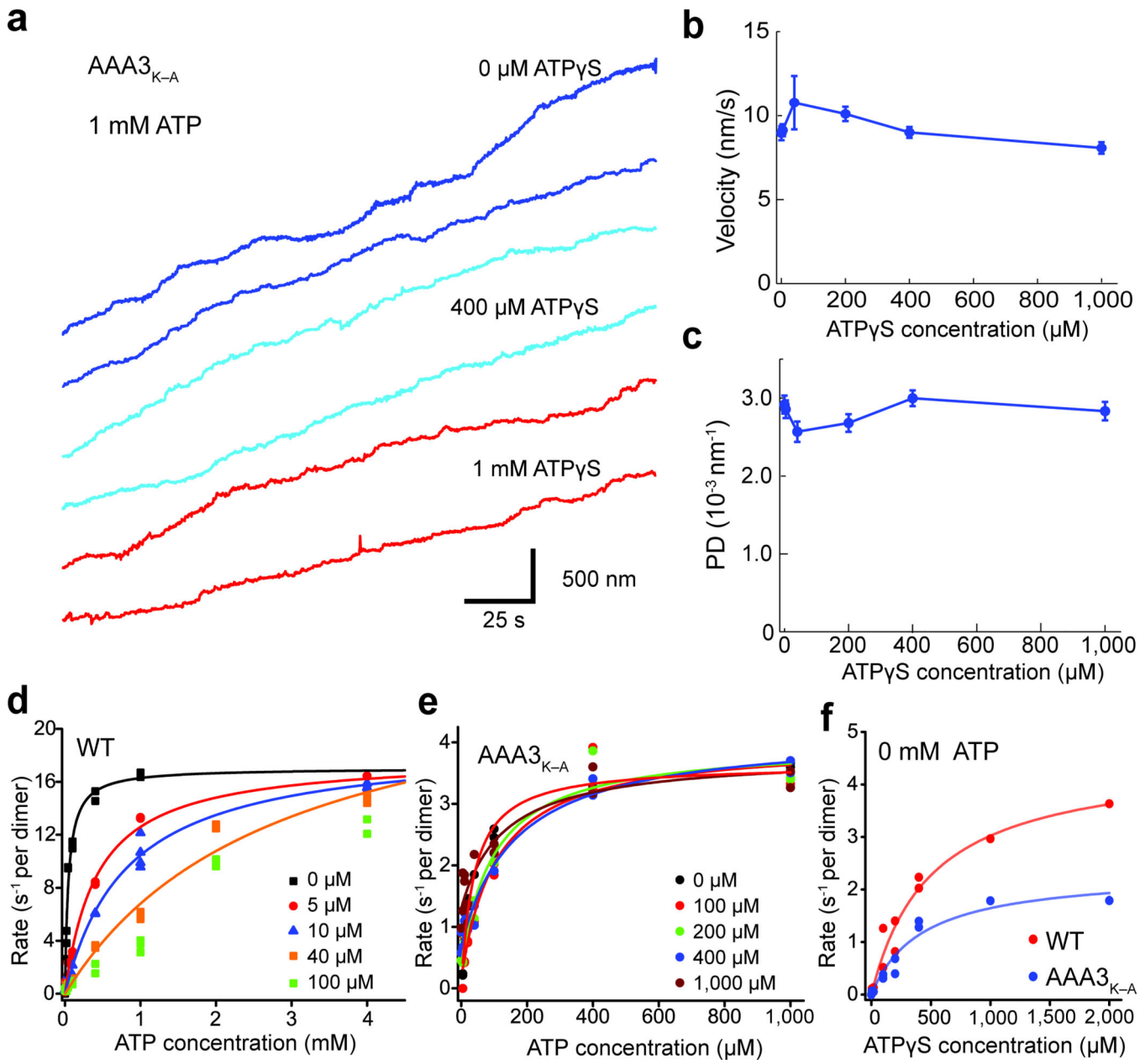

Figure 4. Motility of the AAA3$_{K–A}$ mutant is insensitive to ATPγS

(**a**) Representative traces of QD-labeled AAA3$_{K–A}$ motility at 1 mM ATP and 0 – 1,000 μM ATPγS (*n* = 100). Long pauses are not visible even at 1,000 μM ATPγS. (**b**) The velocity of AAA3$_{K–A}$ as a function of ATPγS concentration. Error bars represent s.e.m of 87–161 traces. (**c**) *PD* of AAA3$_{K–A}$ remains unaffected by ATPγS concentration. Error bars represent s.e.m of *PDs* calculated from 87–161 traces. (**d,e**) ATPase rates of WT (**d**) and AAA3$_{K–A}$ (**e**) at saturating MT concentrations. Colors represent different concentrations of ATPγS. All plotted data are from 3 technical replicates. (**f**) ATPγS hydrolysis rates of WT and AAA3$_{K–A}$ at saturating MTs in the absence of ATP. ATPγS has a weak affinity ($K_{M(ATP\gamma S)}$ = 500 ±110 μM for WT and 425 ± 98 μM for AAA3$_{K–A}$, mean ± 95% c.i.), and a

relatively fast turnover rate ($k_{cat(ATP\gamma S)}$ = 4.52 ± 0.42 s^{-1} for WT and 2.34 ± 0.19 s^{-1} for $AAA3_{K-A}$, mean ± 95% c.i.), consistent with poor inhibition of AAA1.

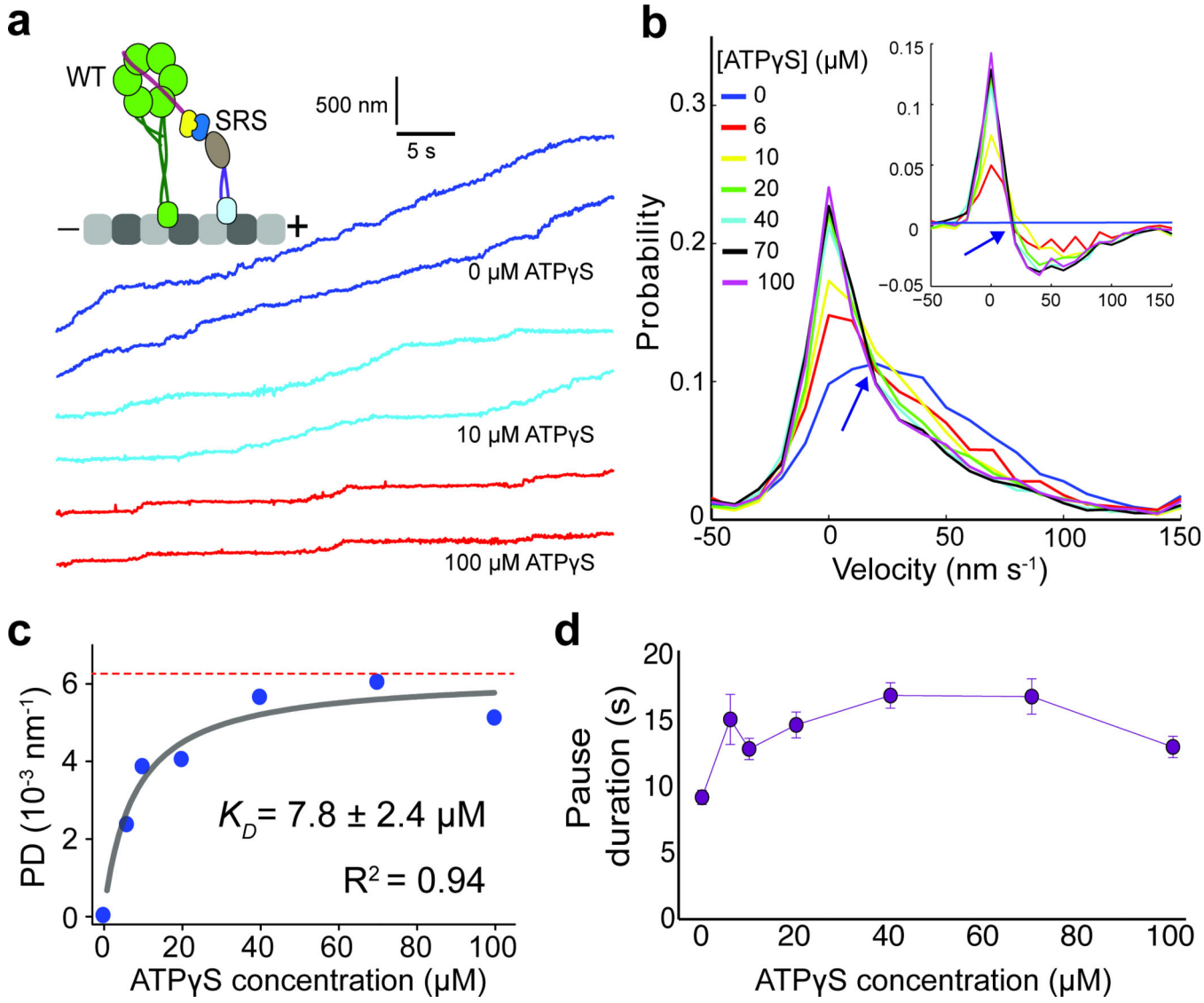

Figure 5. A minimal dynein construct with one AAA+ ring shows two-state pausing behavior

(**a**) Schematic (inset) representing the minimally processive SRS-WT heterodimer. Representative traces of QD-labeled SRS-WT in the presence of 1 mM ATP, and 0, 10, or 100 μM ATPγS show that increasing the ATPγS concentration results in more frequent pauses and slower motility (*n* = 259). (**b**) Normalized histograms of the velocities of SRS-WT over 1 second intervals at varying concentrations of ATPγS. These histograms intersect at 17 nm s^{-1} (blue arrows), consistent with a two-state transition between “fast” and “slow” states. The inset, which shows each histogram with the 0 μM ATPγS histogram subtracted, reveals the velocity distributions of the two populations. (**c**) *PD* of SRS-WT at different ATPγS concentrations. Gray curve represents the fit of the data to the Hill equation with n fixed at 1.0. PD_{MAX} (red dotted line) is 0.0063 ± 0.0004 pauses nm^{-1} (mean ± 95% c.i.). (**d**) Pause duration at different ATPγS concentrations. Error bars represent s.e.m. of 81–277 pauses calculated from 73–259 traces.

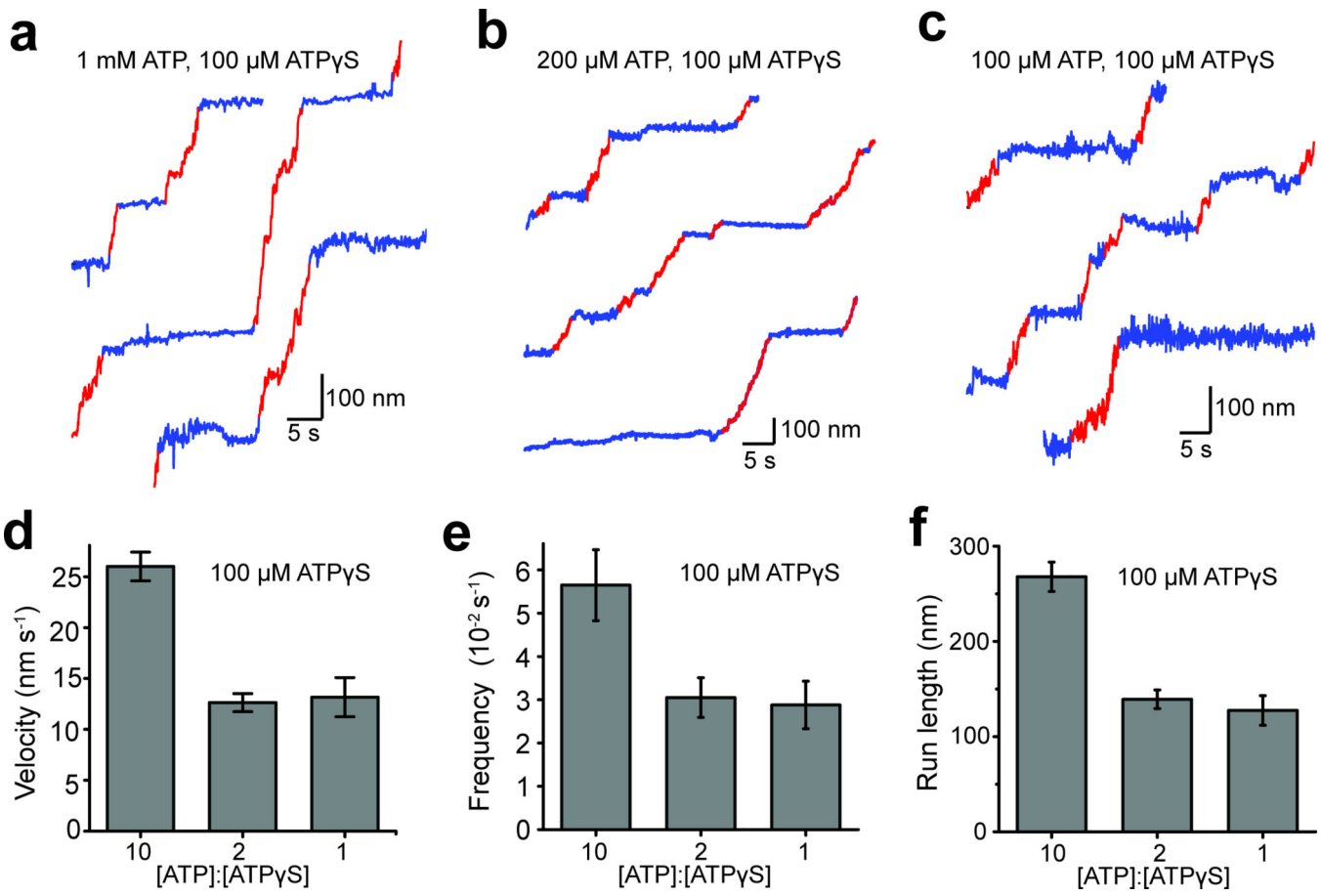

Figure 6. The SRS-WT heterodimer takes long runs between pauses at equimolar concentrations of ATP and ATPγS

(**a,b,c**) Representative traces of SRS-WT motility at 10:1 (**a**), 2:1 (**b**) and 1:1 (**c**) ATP:ATPγS ratios, respectively (*n* = 64, 99, and 117 traces for 100 μM, 200 μM, and 1 mM ATP, respectively). Long runs of fast motility (>15 nm s^{-1}) are shown in red. (**d,e,f**) Velocity (**d**), the frequency of fast runs (**e**) and lengths of fast runs (**f**) of SRS-WT motility at different ratios of ATP to ATPγS. Error bars represent s.e.m. of 64, 99, and 117 traces for 100 μM, 200 μM, and 1 mM ATP, respectively.

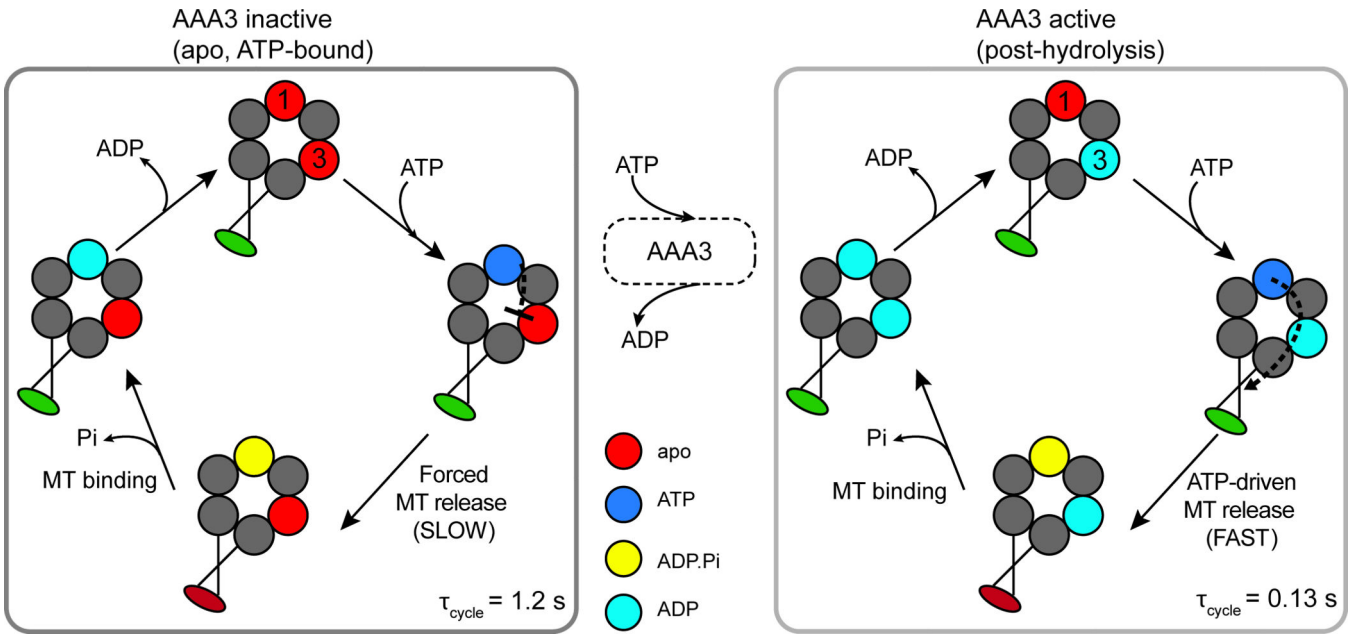

Figure 7.

ATP hydrolysis cycle at AAA1 drives the stepping motility of dynein. (Left) When AAA3 is in the apo state, communication between AAA1 and the MTBD is blocked, resulting in slow, force-dependent MT release, and consequent slow progression through the AAA1 hydrolysis cycle (τ_{cycle} = 1.2 s)[15,18]. (Right) When ATP binds to AAA3 and is hydrolyzed, the allosteric circuit connecting AAA1 and the MTBD is completed. In this state, ATP binding at AAA1 leads to fast release from the MT, and subsequent progression through the AAA1 hydrolysis cycle (τ_{cycle} = 0.13 s). Cycle times are calculated from the bulk ATPase rates per head. This AAA3 controlled switch may play an essential role in repurposing of dynein for intracellular transport (i.e. fast MT release) and anchoring (i.e. slow MT release) functions.